Stochastic simulation of tip-sample interactions in atomic force microscopy

Aleksander Labuda,[1] Martin Lysy,[2] and Peter Grütter[1]
[1]*Department of Physics, McGill University, Montreal, Quebec H3A 2T8, Canada*
[2]*Department of Statistics, Harvard University, Cambridge, Massachusetts 02138-2901, USA*

Atomic force microscopy (AFM) simulators, which are used to gain insight into tip-sample physics and data interpretation, so far have been optimized for modeling deterministic cantilever dynamics. In this article, we demonstrate a method for semi-empirical simulation of the stochastic dynamics of tip-sample interactions. The detection, force, and displacement noises are separately generated directly from their numerically defined power spectral densities and used to simulate a force spectroscopy experiment in water at the mica interface. Mechanical noise of the AFM is shown to dominate over thermal noise of the cantilever upon interaction with the last two hydration layers. © 2012 American Institute of Physics. [http://dx.doi.org/10.1063/1.4745781]

Stochastic noise sets the fundamental limit of force detection in sensitive nanoscale experiments. Thorough investigations of both thermal noise[1,2] and detection noise[3,4] have led dynamic atomic force microscopy to reduce its noise floor and enabled unprecedented experiments such as three-dimensional atomic-resolution of hydration structures at the water-mica interface.[5,6]

Although it is well-known that instrumental vibrations can be detrimental to atomic force microscopy (AFM) experiments, related studies lack scientific appeal because such noise is happenstantial, non-parametric, and its impact on an AFM measurement is difficult to quantify accurately. However, undesirable vibrations of the tip-sample junction can affect the results of an AFM experiment well beyond simple deterioration of image quality.[22]

Given the growing complexity of AFM techniques, numerical simulations of AFM experiments help to understand the effects that instrumental parameters[7,8] and complex cantilever dynamics[9] have on the acquired signals. A recent article[10] outlines the latest developments of the virtual environment for dynamic AFM (VEDA) that is part of the nanoHub.org computation infrastructure as well as presents a thorough literature review of other simulators. So far, VEDA and other simulators are optimized for deterministic calculations of cantilevers dynamics. The next natural step is the inclusion of stochastic cantilever dynamics, as well as vibrations inherent to the instrument and colored detection noise, in order to more accurately reproduce true AFM experiments.

The distinction between these different types of noises was discussed in a recent article,[4] where noise was classified as either detection noise, force noise, or displacement noise. Any noise source falls into one of these categories depending on how it affects the outcome of an AFM experiment and where it enters an AFM simulation, as will be shown later. In this article, these three noise types are simulated separately to assess their respective impact on the measurement of force spectroscopy at the water-mica interface.

Hydration imaging in water[11–13] is performed close to the thermal limits of detection, and the interpretation of acquired data remains controversial.[14–16] Such experiments may benefit from tandem simulations to elucidate sources of instrumental noise and signal artefacts.

We chose to perform our simulation using a 30 μm long 15 μm wide silicon cantilever with a stiffness $k = 10$ N/m. This cantilever was modelled using Sader hydrodynamics[17] for the first eigenmode in water. The frequency-dependent mass $m(\omega)$ and damping $\gamma(\omega)$ were computed from the hydrodynamic function to determine the cantilever impedance[18]

$$\mathcal{C}^{-1}(\omega) = k - m(\omega)\omega^2 + i\omega\gamma(\omega), \quad (1)$$

The natural frequency $\omega_0/2\pi = 350$ kHz and $Q \sim 6$.

The three spectral densities plotted in Fig. 1(a) characterize the noise of the AFM used for the hydration experiment simulation; they were measured/modelled as follows.

The force noise n^2_{force} relates to $\gamma(\omega)$ by the fluctuation-dissipation theorem[1]

$$n^2_{force} = 4k_B T \times \gamma(\omega). \quad (2)$$

This noise scales as $n^2_{force} \sim \omega^{0.52}$ and reaches 1.3×10^{-26} N^2 Hz^{-1} at ω_0. The corresponding cantilever deflection spectral density in the absence of tip-sample interactions is given by $n^2_{force} \times |\mathcal{C}|^2$, as plotted in Fig. 1(a).

The angular detection spectral density of our optical beam deflection system was measured to 5×10^{-19} rad^2 Hz^{-1} at high frequencies,[19] corresponding to a roughly expected 15^2 fm^2 Hz^{-1} of detection noise n^2_{detect} for a 30 μm long cantilever.

The displacement noise was empirically measured on our home-built AFM (Refs. 20 and 21) by pressing a cantilever against a flat sapphire surface, acquiring a power spectral density, and then subtracting the detection noise to obtain n^2_{disp}. A passive vibration isolation table was used. The displacement noise integrates to 36 pm across a [1 Hz, 10 kHz] bandwidth. This measurement compares well with high-end AFMs: our number falls in between the vibrations of the Dimension Icon and Dimension FastScan AFMs (Bruker, Santa Barbara, CA), specified by the manufacturer as 30 pm and 40 pm, respectively, for a bandwidth up to 625 Hz. Our measurement also falls close to the 35 pm specified for the NanoWizard 3 Nanoscience AFM (JPK, Berlin) across a [1 Hz, 1 kHz] bandwidth. This makes the following simulation quantitatively relevant to the majority of AFM users.
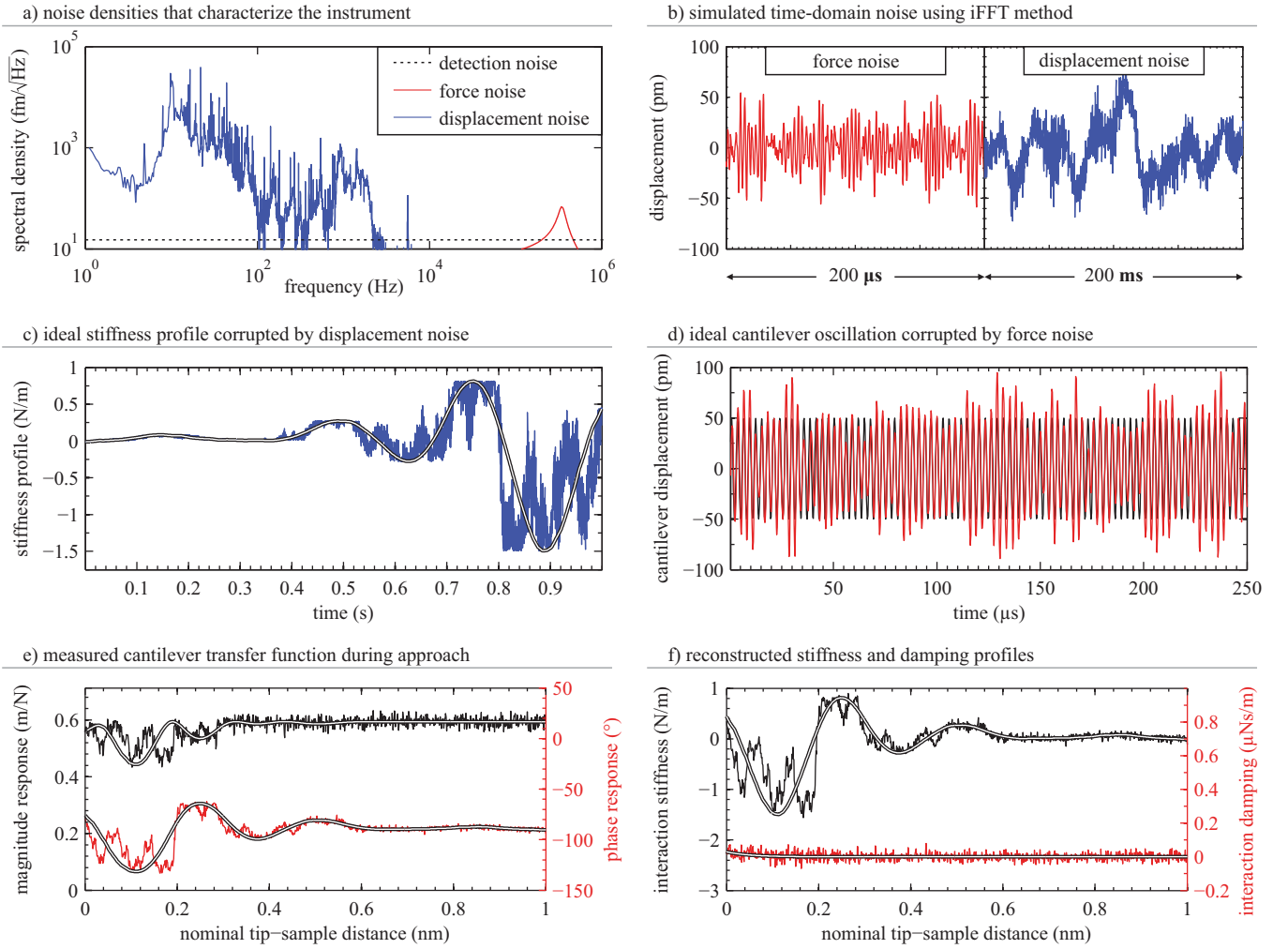
FIG. 1. Outline of the simulated hydration experiment. The spectral densities in (a) were used to simulate time-domain data (b). Displacement noise causes an imperfect stiffness profile seen by the cantilever tip (c), and the force noise adds to the driven cantilever oscillations (d). Detection noise has no measurable impact on the outcome of this experiment. The magnitude and phase response of the cantilever was measured (e), and used to extract the stiffness and damping profiles (f). White lines in (c-e-f) relate to ideal (noiseless) measurements. The results of 100 simulations are available in supplementary material.[27] Note that the "force noise" in this figure was plotted as the cantilever displacement driven by force noise, in order to cast all noise types onto the same units for plotting purposes.

A recent article[22] describes the statistics of the power spectral density (PSD) in the context of noise in AFM, and describes the "iFFT method" for generating time-domain stochastic noise directly from a numerically defined PSD of stationary noise. The iFFT method was used to simulate time-domain noise vectors ϵ_{force}, ϵ_{detect}, ϵ_{disp} from their corresponding PSDs n_{force}^2, n_{detect}^2, n_{disp}^2. These vectors were generated for a duration of 1 s, and the sampling rate was set to 10 MHz to fully resolve the cantilever oscillations. Portions of the simulated ϵ_{force} and ϵ_{disp} are plotted in Fig. 1(b).

The aforementioned cantilever was approached through the oscillatory stiffness profile of the water/mica interface at a rate of $v = 1$ nm/s. The interaction stiffness $k_i(h)$ and damping $\gamma_i(h)$ profiles were taken from measurements in Ref. 6 and used as input for this simulation, where h is the tip-sample distance. Assuming the interaction can be modelled by viscous damping, the interaction impedance

$$\mathcal{J}^{-1}(h, \omega) = k_i(h) + i\omega\gamma_i(h) \qquad (3)$$

adds to the previously described $\mathcal{C}^{-1}$, resulting in the perturbed cantilever impedance $\mathcal{C}_i^{-1}(h, \omega) = \mathcal{C}^{-1}(\omega) + \mathcal{J}^{-1}(h, \omega)$.

Importantly, the displacement noise causes dithering of the stiffness and damping profiles acting on the cantilever tip. Instead of a perfectly linear approach in time, the tip-sample distance h changes as the sum of a linear function and the simulated displacement noise:

$$h(t) = vt + \epsilon_{disp}. \qquad (4)$$

Reparametrizing $\mathcal{J}^{-1}(h, \omega)$ as a function of time takes into account mechanical vibrations, as shown in Fig. 1(c) for the stiffness profile. This reparameterization retains linearity of the system because displacement noise occurs on timescales two orders of magnitude slower than cantilever oscillations.

During an experiment, the quasistatically time-varying transfer function $\mathcal{C}_i(t, \omega)$ is inferred by driving the cantilever with a sinusoidal force at its natural frequency ($\omega_d = \omega_0$). This deterministic driving component is inevitably corrupted by force noise, leading to the total driving force

$$f(t) = F_d \sin(\omega_d t) + \epsilon_{force}. \qquad (5)$$

In the simulation, the response of the cantilever $z(t)$ to this deterministic/stochastic driving force $f(t)$ can be calculated by

$$z(t) = K \sum_{k=0}^{N-1} \mathcal{C}_i(t, \omega_k)\hat{f}(\omega_k)\exp(i\omega_k t) + \epsilon_{detect}, \qquad (6)$$

where $\hat{f}(\omega_k)$ is the Fourier transform of $f(t)$, N represents the size of the dataset (here 10^7), the detection noise ϵ_{detect} was added, and the normalization constant K depends on the specific Fourier transform convention being used. The summation simply represents an inverse Fourier transform; however, the time-dependence of $\mathcal{C}_i(t, \omega_k)$ causes every frequency component $\exp(i\omega_k t)$ to be amplitude and phase modulated before the reconstruction of $z(t)$. Much of the computational burden can be alleviated by only summing over frequencies that are within the demodulation bandwidth of the experiment.

The driving force amplitude $F_d = 200$ pN resulted in an oscillation amplitude of roughly 50 pm prior to tip-sample interaction, allowing us to neglect the convolution of the k_i and γ_i profiles due to finite amplitudes.[23,24] Furthermore, because the damping remained nearly constant during this measurement $(\gamma_i \ll \gamma)$, the thermal force noise was accurately approximated as stationary throughout the experiment, thereby validating the iFFT method[22] used to generate ϵ_{force} earlier.

Next, the magnitude response $|\mathcal{C}_i|$ and phase response $\theta_{\mathcal{C}_i}$ of the perturbed cantilever was calculated by demodulating the deflection signal $z(t)$ with respect to the driving force $f(t)$. The demodulation bandwidth of 1 kHz, resulted in 1000 data points for the 1 sec approach curve. The results are shown in Fig. 1(e).

Finally, both simulated magnitude and phase signals were used to extract estimates of the interaction stiffness k_i and damping γ_i using AM-AFM theory[18]

$$k_i = \frac{\cos\theta_{\mathcal{C}_i}}{|\mathcal{C}_i|} - \frac{\cos\theta_{\mathcal{C}_s}}{|\mathcal{C}_s|}, \text{ and} \qquad (7)$$

$$\gamma_i = -\frac{1}{\omega}\left[\frac{\sin\theta_{\mathcal{C}_i}}{|\mathcal{C}_i|} - \frac{\sin\theta_{\mathcal{C}_s}}{|\mathcal{C}_s|}\right], \qquad (8)$$

where the "s" subscript indicates values measured at the start of the experiment, in the absence of tip-sample interactions. The resulting k_i and γ_i are plotted in Fig. 1(f), where any deviations from the ideal profiles are attributable to noise.

Detection noise contributes to less than 3% of the variability of the measured cantilever displacement in this simulated experiment, making its impact on the extraction of k_i and γ_i negligible. This statement remains true irrespective of the cantilever oscillation amplitude and is valid for demodulation bandwidths up to the corner frequency of the cantilever $(f_0/2Q = 9$ kHz$)$.

Far from the surface, force noise dominates the signal variability. As can be understood from Eq. (2), damping γ is the only free parameter for reducing the thermal force noise in our experiment. Damping scales with the physical size of cantilevers,[25,26] which is why a small cantilever was chosen for this simulated experiment.

Close to the surface, displacement noise overshadows the effects of thermal noise on the measurement of the stiffness profile. Unlike thermal noise, the tip-sample vibrations have a spectral signature that is far from white. This occurs because the bulk of the displacement noise falls below the demodulation bandwidth of 1 kHz. AFM mechanical vibrations are slow, even on the timescale of the 1 s approach. On the other hand, the damping measurement remains limited by thermal noise.

These observations imply that the fundamental limits set by optical shot noise (detection noise) and cantilever thermal noise (force noise) are dominated by mechanical vibrations (displacement noise) for the stiffness measurements of the last two hydration layers in our experiment, while thermal noise overwhelms the damping signal.

Turning on the active vibration isolation of our TS-150 table (Herzan) reduces most of these low-frequency vibrations, and lowers the displacement noise to within a 12-18 pm range on our AFM. This results in a much more faithful measurement of the hydration profile (see supplementary material[27]). Even better performance is expected from a Cypher AFM (Asylum Research, Santa Barbara, CA), which is specified to <15 pm displacement noise across the [0.1 Hz, 1 kHz] bandwidth, and <5 pm in quiet environments. An AFM with such low displacement noise can take full advantage of the thermal noise reduction offered by small cantilevers.

The simulation in this paper assumed a quasistatically time-varying dynamical steady-state of the system with a stationary thermal force noise. These properties linearize the system, allowing for convenient, yet accurate, approximations that facilitated this simulation. We foresee that more sophisticated AFM simulators will adopt the stochastic simulation principles presented here and extend simulations to non-equilibrium dynamical experiments performed close to the fundamental limits of detection.

[1]C. D. F. Honig, M. Radiom, B. A. Robbins, J. Y. Walz, M. R. Paul, and W. A. Ducker, Appl. Phys. Lett. **100**, 053121 (2012).
[2]A. Gannepalli, A. Sebastian, J. Cleveland, and M. Salapaka, Appl. Phys. Lett. **87**, 111901 (2005).
[3]T. Fukuma, T. Ichii, K. Kobayashi, H. Yamada, and K. Matsushige, Appl. Phys. Lett. **86**, 034103 (2005).
[4]A. Labuda, J. R. Bates, and P. H. Grütter, Nanotechnology **23**, 025503 (2012).
[5]T. Fukuma, Y. Ueda, S. Yoshioka, and H. Asakawa, Phys. Rev. Lett. **104**, 2 (2010).
[6]A. Labuda, K. Kobayashi, D. Kiracofe, K. Suzuki, P. H. Grütter, and H. Yamada, AIP Adv. **1**, 022136 (2011).
[7]L. Nony, A. Baratoff, D. Schär, O. Pfeiffer, A. Wetzel, and E. Meyer, Phys. Rev. B **74**, 1 (2006).
[8]M. Gauthier, R. Pérez, T. Arai, M. Tomitori, and M. Tsukada, Phys. Rev. Lett. **89**, 146104 (2002).
[9]J. Melcher, C. Carrasco, X. Xu, J. L. Carrascosa, P. José de Pablo, and A. Raman, Proc. Natl. Acad. Sci. U.S.A. **106**, 13655 (2009).
[10]D. Kiracofe, J. Melcher, and A. Raman, Rev. Sci. Instrum. **83**, 013702 (2012).
[11]T. Fukuma, K. Kobayashi, K. Matsushige, and H. Yamada, Appl. Phys. Lett. **87**, 034101 (2005).
[12]B. W. Hoogenboom, H. J. Hug, Y. Pellmont, S. Martin, P. L. T. M. Frederix, D. Fotiadis, and A. Engel, Appl. Phys. Lett. **88**, 193109 (2006).
[13]S. de Beer, D. van den Ende, and F. Mugele, Appl. Phys. Lett. **93**, 253106 (2008).
[14]G. B. Kaggwa, J. I. Kilpatrick, J. E. Sader, and S. P. Jarvis, Appl. Phys. Lett. **93**, 011909 (2008).
[15]S. D. Beer, W. K. D. Otter, D. V. D. Ende, W. J. Briels, and F. Mugele, Europhys. Lett. **97**, 46001 (2012).
[16]S. O'Shea, Phys. Rev. Lett. **97**, 179601 (2006).
[17]J. E. Sader, J. Appl. Phys. **84**, 64 (1998).
[18]A. Labuda and P. Grütter, Langmuir **28**, 5319 (2012).
[19]A. Labuda and P. H. Grütter, Rev. Sci. Instrum. **82**, 013704 (2011).

[20]A. Labuda, W. Paul, B. Pietrobon, R. B. Lennox, P. H. Grütter, and R. Bennewitz, Rev. Sci. Instrum. **81**, 083701 (2010).

[21]A. Labuda, K. Kobayashi, Y. Miyahara, and P. Grutter, Rev. Sci. Instrum. **83**, 053703 (2012).

[22]A. Labuda, M. Lysy, W. Paul, Y. Miyahara, P. Grütter, R. Bennewitz, and M. Sutton, Phys. Rev. E **86**, 031104 (2012).

[23]F. J. Giessibl, Appl. Phys. Lett. **78**, 123 (2001).

[24]J. E. Sader and S. P. Jarvis, Appl. Phys. Lett. **84**, 1801 (2004).

[25]D. A. Walters, J. P. Cleveland, N. H. Thomson, P. K. Hansma, M. A. Wendman, G. Gurley, and V. Elings, Rev. Sci. Instrum. **67**, 3583 (1996).

[26]M. B. Viani, T. E. Schäffer, A. Chand, M. Rief, H. E. Gaub, and P. K. Hansma, J. Appl. Phys. **86**, 2258 (1999).

[27]See supplementary material at http://dx.doi.org/10.1063/1.4745781 for simulated experiments with both the Herzan table turned on and off.